Journal of the Meteorological Society of Japan, Vol. 73, No. 2B, pp. 549–556, 1995

NOTES AND CORRESPONDENCE

Tentative Utilization of a Raindrop Size Distribution Meter Specially Designed for the Observation of Tropical Precipitation in the TOGA/COARE Project

By Ken-ichiro Muramoto, Takashi Fujiki

Faculty of Engineering, Kanazawa University, Kanazawa 920, Japan

Masaki Kaneda and Tatsuo Endoh

Institute of Low Temperature Science, Hokkaido University, Sapporo 060, Japan

(Manuscript received 31 August 1994, in revised form 27 February 1995)

Abstract

To offer precise data for a more quantitative analysis of the data obtained by the dual Doppler radar system, a specially designed raindrop size distribution meter was utilized at Manus Island, Papua New Guinea, in the TOGA/COARE project. The measuring device consists of an optical system with a light source and two video cameras. The raindrops that fall through a slit are illuminated against a uniform surface light source by means of a frosted glass plate immediately next to them and their shadow images are photographed by two video cameras with different shutter speeds for simultaneously measuring size and velocity of fall of the same raindrop. Fall velocity is used to examine the size measured and provides a highly reliable measurement of size for even the smaller raindrops.

In this paper, two different types of size distribution of raindrops are shown by a single modal Gamma function and a bimodal distribution corresponding to relatively weak and relatively strong convective clouds, respectively. The bimodal case is discussed in comparison with the radar data analyzed in a few instances of a series of rainfall periods and some of the results provide possible evidence for the warm-rain mechanism and evaporation processes.

1. Introduction

In the tropical region of the TOGA-COARE-IOP network in the west Pacific Ocean, a dual Doppler radar observation was carried out to clarify the real features of convective cloud systems over the warm-pool area of the southern oscillation phenomenon on Manus Island, Papua New Guinea, from November 1992 to January 1993, as described in more detail by Uyeda *et al.* (1995). To perform the radar analyses with quantitative precision and to evaluate accurately the amount of precipitation from radar echo intensity, it is necessary for the size distributions of raindrops to be measured simultaneously at the ground.

In that region, from the sounding data at Momote airport on Manus Island (2°03′S, 147°26′E, 2 m asl) during the observational period (Nov. 1992–Jan. 1993), the heights of the cloud base were around 1000 m. However, some bases were occasionally observed up to 3000 m or more (Takahashi *et al.*, 1995). In addition, since the air temperature or saturation vapor pressure is higher than that in middle-latitude regions, raindrop evaporation is expected to take place actively below the cloud base down to the earth's surface and to deform the original size distribution of raindrops to that observed at the ground.

To date, many kinds of raindrop size distribution meter have been developed. However, their sensitivity for small size, (diameter < 0.7 mm) is not satisfactory for measuring the size distribution of raindrops. Originally, dyed filter paper was used by many researchers, such as Marshall and Palmer (1948) and Mason and Andrew (1960). Filter paper

was exposed to rainfall and the number of stains was counted and measured to determine the size distribution. However, this method is too laborious and inefficient to determine features of a cloud system on the mesoscale. Bowen and Davidson (1951) used a horizontal wind tunnel to classify the sizes of falling raindrops. A different method, originally used by Schindelhauer (1925) and later improved by Maulard (1951), counted and measured the number and size of falling raindrops by the electrical pulses and amplitudes which they generated upon striking a microphone diaphragm. Cooper (1951) presented a balloon-borne version of the microphone-type instrument to measure raindrop size and rain water content at different altitudes. These methods have been improved and used extensively and the commercial instrument is known as a "Disdrometer." However, the disdrometer's measuring capability is not satisfactory as it measures lower than reasonably expected frequencies for smaller ranges in the size distribution of raindrops, although the raindrops were at well developed stages. Some methods of optical path interception have been tried, developed by Mason and Ramanadham (1953), and later improved by Dingle and Schulte (1962) to increase the sampling volume without interception of the raindrop images.

Recently, an optical disdrometer had been developed by Stow and Jones (1981) and utilizing it the arrival rate of raindrops was measured by Hosking and Stow (1987). Furthermore, ground-based, high-resolution measurements had been performed by Hosking and Stow (1987b) and they had deduced the spatial and temporal distribution of rainfall.

A tentative utilization of a specially designed raindrop size distribution meter was carried out at one of the radar sites in the dual Doppler radar observation system, at Momote airport, with the location as described by Uyeda *et al.* (1995) and shown as the origin (center) in the coordinate of radar PPI frame schematics in Figs. 6 and 7. Although the amount of data was only small, and the duration observed successfully was unfortunately only short, the observational methods developed in the present work and some remarkable size distributions of raindrops with analyses of radar data are reported in the following sections.

2. Methods

The measuring system and hardware diagram are shown in Fig. 1. The apparatus consists of a halogen light source (IWASAKI, JAWO 500W) and two CCD-video cameras (SONY XC-77RR). Images of raindrops that have fallen through a slit are observed on a frosted glass plate as enlarged shadow figures. One of the cameras has a high shutter speed of 1/20000 (±1 %) second for measuring the dimensions of the raindrop. The other has a 1/2000

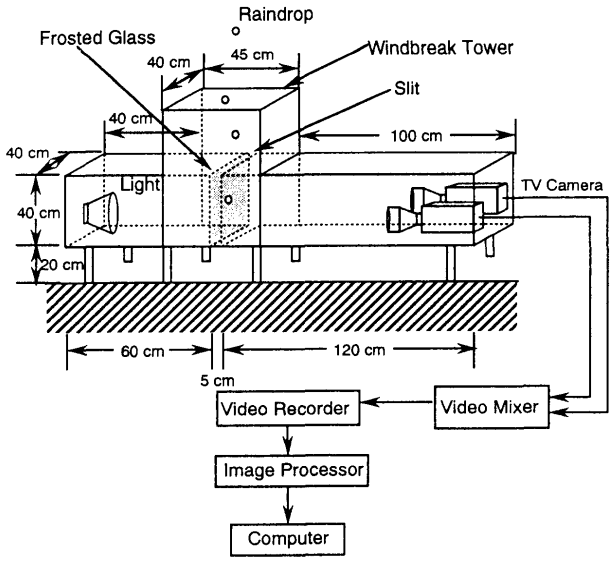

Fig. 1. Schematic for the simultaneous measurement of the size and fall velocity of raindrops.

(±1 %) second shutter speed for measuring the fall velocity of the same raindrop for an occasional examination of the empirical relationship between terminal velocity and dropsize as reported by Gunn and Kinzer (1949). The volumes of the spaces photographed inside the illuminated area depend on the frame ranges of the zooming lenses (TAMRON SP-19AH), and are limited practically by 32 mm (Width) × 51.2 mm (Height) × 50 mm (Depth), and 48 mm (Width) × 128 mm (Height) × 50 mm (Depth) into the high- and low-speed cameras respectively, as shown in Fig. 2. Two images of a raindrop and the vertical displacement of the same raindrop were taken by two different video cameras simultaneously every 1/30 second and combined again by a video mixer to form a single pair of images in order to synchronize the time taken. The width of the slit was empirically selected and limited to 5 cm in order to obtain the image of a raindrop at least every frame, to eliminate the interception of two or more raindrops taken in the same frame, and to minimize and ignore the differences of the falling positions of the raindrops against a long working distance of 120 cm as shown in Fig. 1.

The images of the raindrops were converted into digital form with an image analysis board installed on a personal computer. Digitized images consisted of a 512 × 512 pixel array, each pixel holding a designated gray value ranging from 0 to 255. The photographs taken were composed of two kinds of regions that occupy different gray-level ranges. All parts of the raindrop images were darker than the background image, and the pixels with gray levels darker than the background were considered as part

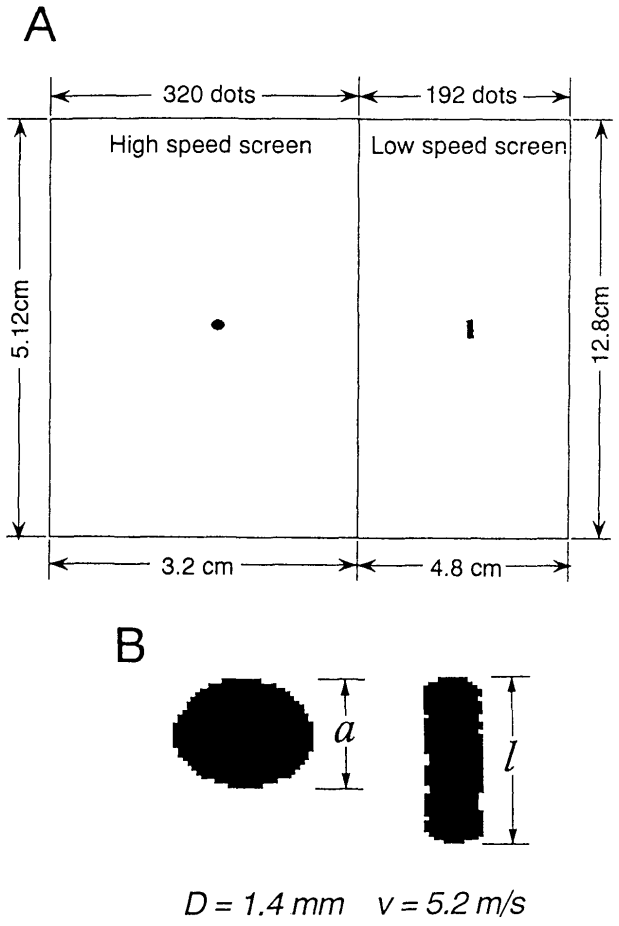

Fig. 2. An example of images observed by two video-cameras, and the measured dimensions for size and falling velocity determination. a: vertical dimension of the image of raindrop taken by the high-speed camera. l: vertical dimension of the image of falling displacement of a raindrop taken by the low-speed camera

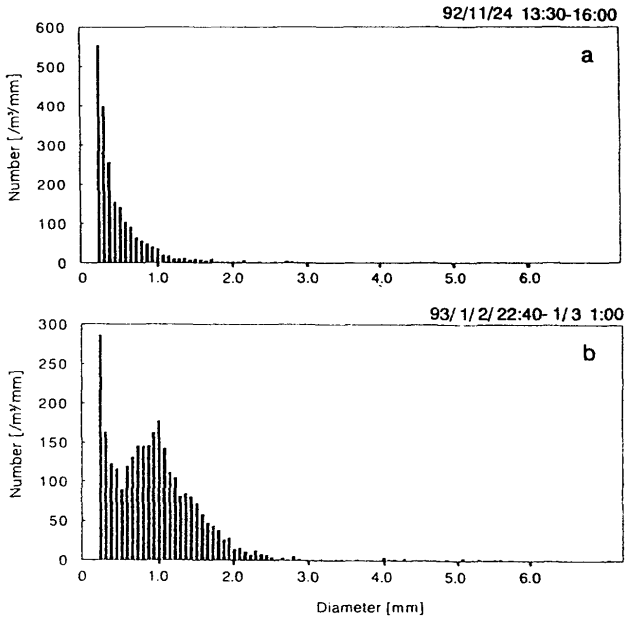

Fig. 3. Two diffent examples of the size distribution of raindrops. a: 13:30–14:30 24 November 1992 (with stratified-type echoes) b: 22:40–00:30 2 January 1993 (with convective-type echoes)

of the raindrops. The pictures of the raindrops could thus be segmented.

Each pair of binary images of the raindrops shows high and low speed projections consisting of pixels as in the example shown in Fig. 2. The area of cross section A of a raindrop is obtained from the number of pixels inside the region of the high speed projection. The equivalent diameter D of the raindrop is calculated from the area of cross section A, *i.e.*, $D = 2 \cdot (A/\pi)^{\frac{1}{2}}$. The smallest size detected is expected to be 0.2 mm in diameter since the dimension of a pixel is 0.1 mm. The greatest size able to be measured is that naturally occuring of 6 mm in diameter. The principle of the measurement of this work may be applied to the spherical or vertical-axis symmetric solid precipitation particles, for example smaller round graupel, frozen raindrops, and hail pellets less than 1 cm in diameter, but should not be applied to asymmetric particles, *e.g.* snowflakes and conical graupel.

Since each falling raindrop produced a short streak during the 1/2000 second time interval, its velocity is calculated from the vertical length l. Assuming that each raindrop is spherical or a rotating ellipse, the vertical dimension a is calculated by the image of high speed projection and composed of the vertical displacement during the projection. The example of the image of a raindrop shown in Fig. 2 is slightly deformed and flattened. Then, using the difference of these falling distances $(l - a)$ for (1/2000) second, the fall velocity v is computed by $v = (l - a)/(1/2000)$. The lowest fall velocity detected is down to 56 cm/sec due to a pixel length of 0.25 mm. The greatest fall velocity detectable is almost 12 m/sec. The principle of the measurement in this work may be applied to all kinds of solid precipitation particles whose fall velocities are lower than 12 m/sec. The number concentration is also computed from the number of raindrops in the space photographed.

The reliable value of the minimum size of the raindrops detected was 0.3 mm in diameter because of a greater deviation than 10 % in the calibration when comparing the empirical curve of Gunn and Kinzer (1949) with the observed fall velocity, which was assumed to be easily affected by air motion due to wind in the apparatus.

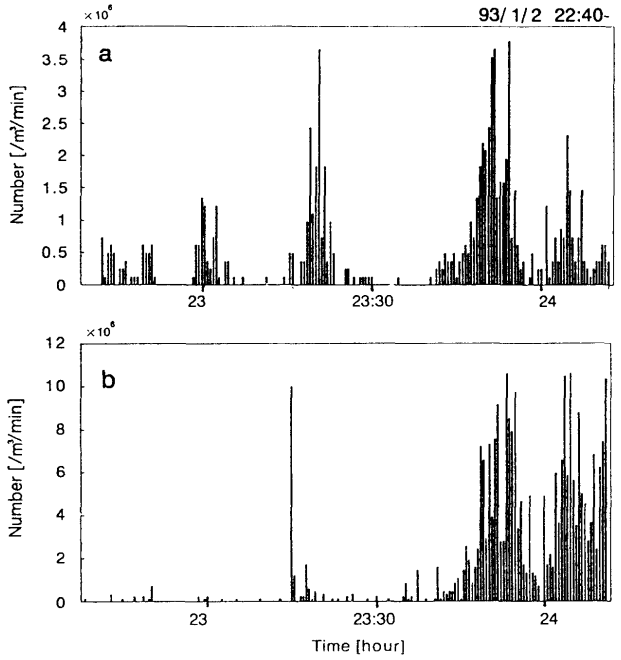

Fig. 4. Temporal changes of the number concentration of raindrops in the diameter range smaller (upper) and larger (lower) than 0.5 mm. The duration is as for the case in Fig. 3b.

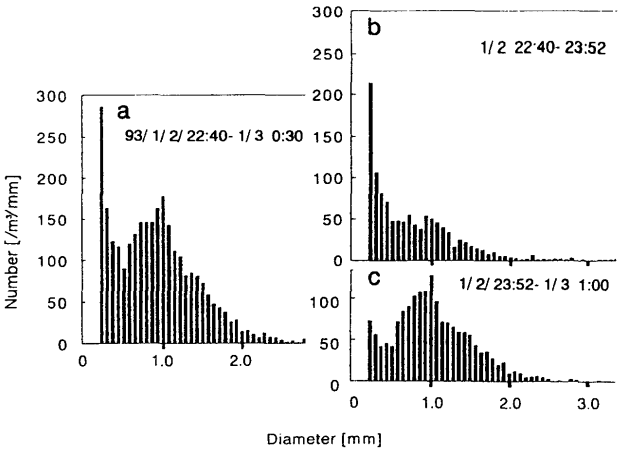

Fig. 5. Comparison of size distributions of raindrops between two stages over the duration of Fig. 3b. a: (reference) 22:40–00:30 b: 22:40–23:52 and c: 23:52–00:30 in 2, 3 January 1993.

3. Results

Two different types of the size distribution of raindrops are shown, as in the examples measured in Fig. 3, where the size distributions of 3a and 3b are constructed by 4738 and 5931 raindrops with average sampling error of 3 and 7 % over the diameter range of 0.3–1.0 mm and 1.0–6.0 mm, respectively. Cases 3a and 3b correspond to the radar echoes of a weak and uniformly stratified system and to a strong convective one, respectively. In the case of Fig. 3a, it is seen that the shape of distribution is in that of an exponential function, *i.e.* Gamma distribution and that the average diameter is smaller than 1 mm with the maximum diameter ranging up to 3 mm with extremely low frequency. Conversely, in Fig. 3b, it is noted that the shape of distribution is bimodal. The secondary mode diameter is approximately 1 mm and the maximum diameter is up to 5 mm or greater, this being a common trait in tropical rainfalls. It should be noted that the total number of raindrops in the former case is much larger than that in the latter, and *vice-versa* in terms of the total mass of rain water. These differences are easily seen by comparing the different types of radar echoes described above.

In Fig. 4, two temporal changes of the number concentration of raindrops are shown. A value of 0.5 mm in diameter is used to distinguish between larger and smaller raindrops and the resulting comparison is as shown. Note that this value is around the value in the saddle point between the modes in Fig. 3b. The figure shows that the smaller raindrops were observed to fall over the duration. In the final stage, however, it is noted that larger ones also join with them. It may be expected that two different kinds of size distributions would make up a bimodal distribution of raindrops summarized over the whole duration. To verify this, a transitional time of drop size shifting from smaller to larger modes was found to be at 23:52, which clearly divided the duration into two characteristic rainfalls of earlier and later stages. These two different size distributions corresponding to the stages are shown in Figs. 5b and 5c, where size distributions of 5b and 5c are constructed by 2393 and 3538 raindrops with the same sampling errors as described in Fig. 3 and compared with the shape of distribution over the whole duration of Fig. 5a. The shapes of size distributions were generally exponential or normal in the stages where small and large raindrops predominated, respectively. From the shape of the size distribution in Fig. 5c in comparison with that in Fig. 5b, it is considered that lower frequencies over size ranges smaller than 0.5 mm are caused by the effects of evaporation erosion due to downdraft or coalescence loss, and the interception loss of the inner periphery of the slit by the strong wind expected to accompany the convective-type rainfall. On the other hand, it is reasonable to consider that obvious increasing frequencies in the manner of a normal distribution mode around 1.0 mm in diameter are caused by the coalescence growth of raindrops in a tropical warm-rain mechanism.

The characteristic properties of size distribution in these tropical areas could not be discussed quan-

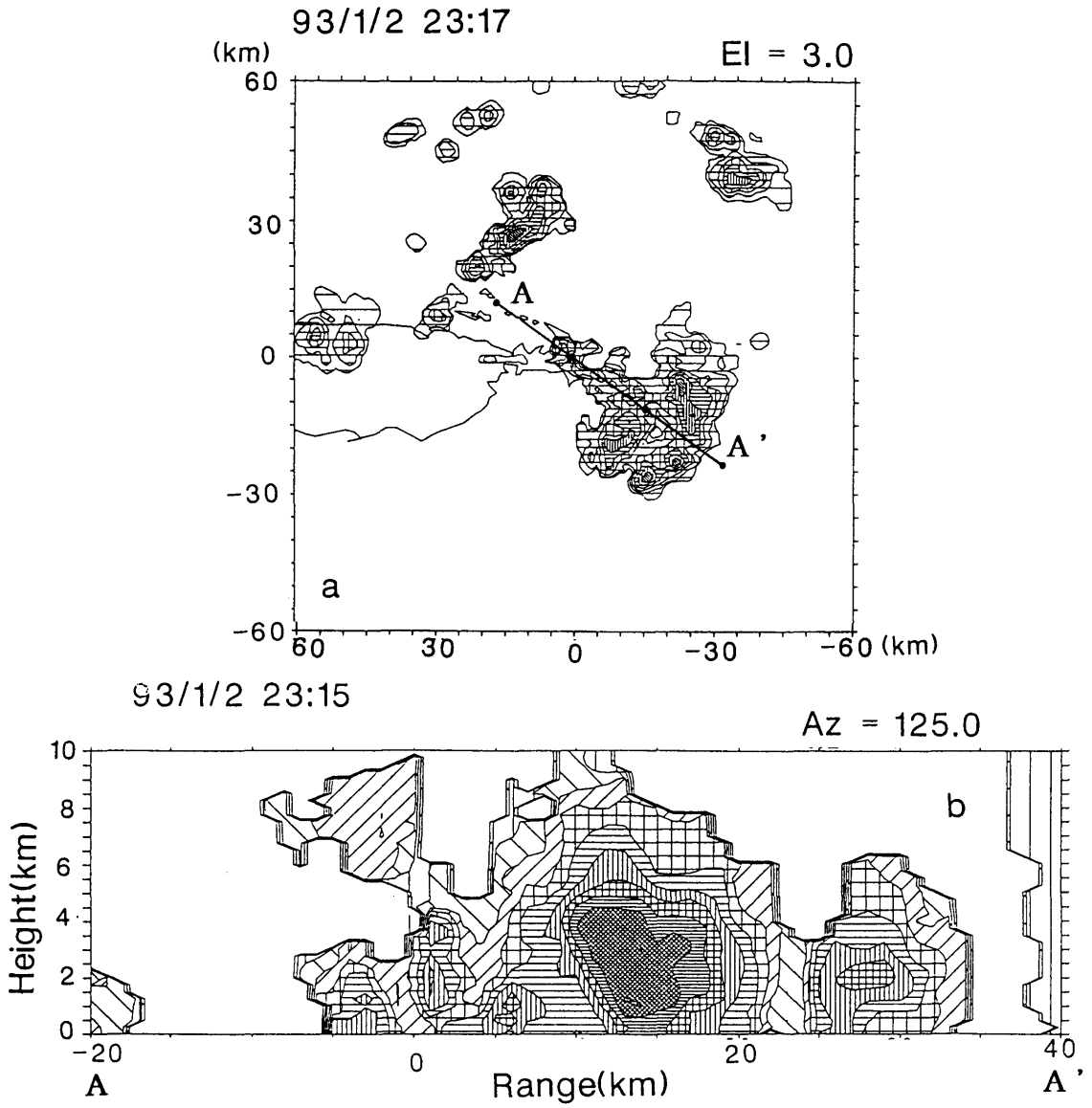

Fig. 6. Radar echo intensity in PPI (EL = 3.0°) and RHI (AZ = 125.0°). a: 23:17 b: 23:15 on the 2nd January 1993. The cross section of the RHI is indicated by AA′ in the PPI, and cross-hatched domain in the RHI indicates the maximum echo intensity of 36 dBZ, from where contour lines are indicated with a decreasing interval of 3 dBZ.

titatively because of insufficiency of the number of the observational cases.

4. Applications for analyses of radar data

The size distribution of the precipitation may be used to provide more extended arguments and considerations for the analyses of radar observations. The following discussion attempts to explain the results obtained in the present work by comparing with the radar data.

Two pairs of radar echoes are shown in the PPI and RHI in the earlier and later stages in Figs. 6 and 7. It may be seen from Figs. 6a to 7a that the direction of the displacement of the whole echo system is deduced to turn toward the azimuth of 125 degrees. According to the echo motion, the horizontal distribution of echoes expands somewhat in the manner of the transversal mode of cloud alignment. The observation site is located on the origin of the coordinate axes (0 km, 0 km), or the center of the PPI schematics. The rainfalls are seen to be brought by somewhat diffusive trace echoes extending from one of the rear side portions of the transversal echo system in a northwesterly motion in both schematics of Fig. 6. From the RHI schematic along the echo motion in Fig. 6b at the observation site, it is seen that a vertically-limited domain of the strongest echo intensity exists aloft at a height

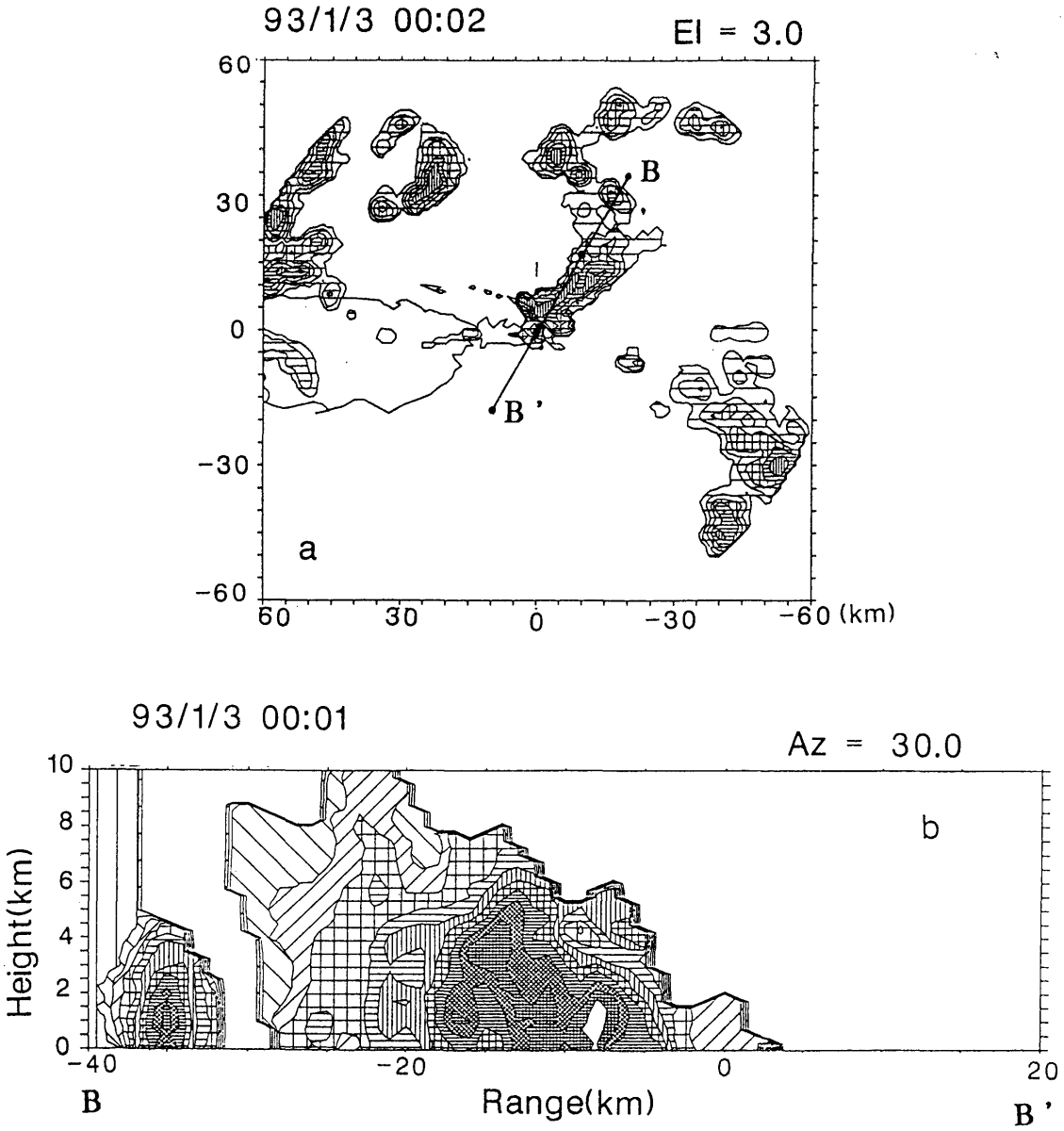

Fig. 7. Radar echo intensity in PPI ($EL = 3.0°$) and RHI ($AZ = 30.0°$). a: 00:02 b: 00:01 on the 3rd January 1993. The cross section of the RHI is indicated by BB′ in the PPI, and a white domain in the RHI indicates maximum echo intensity of 42 dBZ, from where contour lines are indicated with a decreasing interval of 3 dBZ.

of approximately 2 km at a position of 15 km on the horizontal axis. From there, some weak echoes extend backward, fall, and then reach the observation site, indicated on the position as 0 km on the horizontal axis of the RHI schematic. It is thought that these trace echoes bring rainfall at the surface in the earlier stage, as described in Figs. 4 and 5.

On the other hand, the next transversal echo alignment in Fig. 6a is seen to develop and arrive over the observation site with the southwest end of the echo alignment in Fig. 7a. From the RHI schematic along the core axis of the transversal alignment forward on an azimuth of 30 degrees in Fig. 7b, it is observed that the strongest echo domain stands vertically and reaches the earth's surface a few km northeast of the observation site. It may also be considered that one part of these strong echoes brings the heavy rainfall in the later stage of Fig. 4. Regarding the discrepancies of the position of the strong echoes and the heavy rainfall observed at the site, it might be supposed from the strong echo on the site shown in Fig. 7a that if we had performed the radar observation in the scanning mode of RHV (RHI) along the direction of the echo motion we could expect that a quite strong echo would be obtained right at the site.

In the vertical structures of the echoes in RHI in Fig. 6b, it is apparent that the vertical domain of the strongest intensity of echo existed and did not descend to the surface in the earlier stage of the rainfall with the small raindrops shown in Fig. 5b. On the other hand, it is easily seen that the vertical domain of the strongest intensity of echoes extended onto the earth's surface in the later stage of the rainfall with the large raindrops shown in Fig. 5c.

From the sounding curve on the observation site at the most immediate time, the freezing level (0°C) was at a height of 4.0 km. Therefore, the increases in echo intensity with decreasing height from 4.0 km in Figs. 6b and 7b are thought to correspond to the "bright band" effect. Although, according to a private communication (T. Takahashi of Kyushu University), these effects were expected to continue up to the 10°C level, corresponding to 2.5 km in the present case. The vertical distribution of the domains of the strongest intensity of echo are seen to extend over the lower levels, develop with decreasing level, and then arrive at the earth's surface in the later stage of the rainfall at the position of −8 km on the horizontal axis in the RHI of Fig. 7b. Fujiyoshi *et al.* (1994) had supposed that such enhancements of echo intensity were caused by coalescence growth taking place, namely, the "warm-rain mechanism". The results of the present work show simultaneous measurements of an increase in frequencies around 1.0 mm in diameter on the size distribution of raindrops in Fig. 5c and an enhancement of the echo intensity of 20 dBZ or more relative to the surroundings, even below a height of 2 km at the position of −8 km on the horizontal axis in the RHI of Fig. 7b. Therefore these simultaneous records are thought to provide important evidence for their hypotheses.

5. Concluding remarks

The size distribution of raindrops in tropical precipitation were measured by a two-video camera method specially designed for high reliability with smaller ranges down to 0.3 mm in diameter combined with dual Doppler radar observation during the TOGA/COARE-IOP in Manus, Papua New Guinea.

Although the smallest drop size detected is 0.2 mm or smaller, the reliable value of the minimum size of the raindrops detected was 0.3 mm in diameter because of a greater than 10 % deviation in the calibration when compared to the empirical curve of Gunn and Kinzer (1949). The observed fall velocity was assumed to be affected by air motion due to wind in the apparatus.

Two different types of examples of the size distribution of raindrops were obtained by a tentative utilization of the apparatus. These are single exponential and bimodal distributions, corresponding to a uniformly-stratified-type echo, and a convective-type echo of cloud systems observed by the radar.

Fortunately, the bimodal distribution was able to be simply divided by a time-partition method with a single transition time. Single exponential and normal distribution functions were fitted in the earlier and later stages, respectively. It may be noted that the former and latter distributions respectively correspond to a stratiform rainfall and shower-type rainfall from convective clouds. It may be considered from the analyzed radar data that the latter is caused by the coalescence mechanism.

However, the number of cases and the volume of data obtained was not very large. Furthermore, it is expected that their utilization will be extensively applied in quantitative analyses of dual Doppler radar data.

Acknowledgments

The authors express their thanks to the National Weather Service, Papua New Guinea, for their cooperation. We are grateful to the Japan Marine Science and Technology center for their assistance in the transportation of equipment to Manus Island, Papua New Guinea. One of the authors, K. Muramoto is grateful to Mr. M. Furukawa of Kanazawa University for the development of this measuring system. Further, T. Endoh is also grateful to Dr. H. Uyeda, for his substantial support for this study and Dr. Y. Tachibana and Dr. S. Satoh for their cooperation in the radar observation. We would like to thank Professor Kensuke Takeuchi of the Institute of Low Temperature Science, Hokkaido University, Professor Akimasa Sumi of the Center for Climate System Research, University of Tokyo and Associate Professor Y. Fujiyoshi of the Institute for Hydrospheric-Atmospheric Science, Nagoya University for their encouragement throughout this study.

This study was supported by the Grant-in-Aid for Scientific Research from the Ministry of Education, Science and Culture of Japan (No. 06NP021).

References

Bowen, E.G. and K.A. Davidson, 1951: A raindrop spectrograph. *Qurt. J. Roy. Meteor. Soc.*, **77**, 445–450.

Cooper, B.F., 1951: A balloon-borne instrument for telemetering raindrop size distribution and rainwater content of cloud. *Aust. J. Appl. Sci.*, **2**, 43–48.

Dingle, A.N. and H. Schulte, 1962: A research instrument for the study of raindrop-size spectra. *J. Appl. Meteor.*, **1**, 48–59.

Fujiyoshi, Y., G. Biao, H. Uyeda, K. Takeuchi and A. Sumi, 1994: Dual Doppler radar observation of a tropical rainband developed from two small convective clouds. *Proc. 2nd Korea-Japan Joint Workshop for TOGA-COARE*, 1993, 75–82.

Gunn, R. and G.D. Kinzer, 1949: The terminal velocity of fall for water droplets in stagnant air. *J. Meteor.*, **6**, p. 243.

Hosking, J.G. and C.D. Stow, 1987: The arrival rate of raindrops at the ground. *J. Clim. Appl. Meteor.*, **26**, 433–442.

Hosking, J.G. and C.D. Stow, 1987b: Ground-based, high-resolution measurements on the spatial and temporal distribution of rainfall. *J. Clim. Appl. Meteor.*, **26**, 1530–1539.

Marshall, J.S., W.M. Palmer, 1948: The distribution of raindrops with size. *J. Meteor.*, **5**, 165–166.

Mason, B.J. and J.B. Andrew, 1960: Drop-size distributions from various types of rain. *Quart. J. Roy. Meteor. Soc.*, **86**, 346–353.

Mason, B.J. and R. Ramanadham, 1953: A photoelectric raindrop spectrometer. *Quart. J. Roy. Meteor. Soc.*, **79**, 490–495.

Maulard, J., 1951: Mesure du nombre de gouttes de pluie. *J. Sci. Meteor.*, **3**, 69–74.

Schindelhauer, H., 1925: Versuch einer registrierung der trophenzahl bei regenfaellen. *Met. Z.*, **42**, 25–30.

Stow, C.D. and K. Jones, 1981: A self-evaluating disdrometer for the measurement of raindop size and charge at the ground. *J. Appl. Meteor.*, **20**, 1160–1176.

Takahashi, T., K. Suzuki, M. Orita, M. Tokuno and R. de la Mar, 1995: Videosonde observations of precipitation processes in equatorial cloud clusters. *J. Meteor. Soc. Japan*, **73**, 509–534.

Uyeda, H., Y. Asuma, N. Takahashi, S. Shimizu, O. Kikuchi, A. Kinoshita, S. Matsuoka, M. Katsumata, K. Takeuchi, T. Endoh, M. Ohi, S. Satoh, Y. Tachibana, T. Ushiyama, Y. Fujiyoshi, R. Shirooka, N. Nishi, T. Tomita, H. Ueda, T. Sueda and A. Sumi, 1995: Doppler radar observations on the structure and characteristics of tropical clouds during the TOGA-COARE IOP in Manus, Papua New Guinea — Outline of the observation —. *J. Meteor. Soc. Japan*, **73**, 415–426.

TOGA/COARE プロジェクトの熱帯降雨観測で開発した雨滴の粒径分布測定装置の試験的使用

村本健一郎・藤城孝史

(金沢大学工学部)

金田昌樹・遠藤辰雄

(北海道大学低温科学研究所)

降雨のレーダ・データを定量的に解析する上で雨滴の粒径分布が得られると有効である。そのためTOGA/COAREプロジェクトで実施された2台のドップラーレーダによるデュアル観測においても、このために特別に開発された雨滴の粒径分布の測定装置がパプア・ニューギニャのマヌス島で使用された。本装置は1つの光源と2台のビデオ・カメラの光学系から成っており、その間を、上部のスリットを通って落下する雨滴のイメージを擦りガラスで一様にした面光源を背景とする影の像として捉え、それをデジタル処理するものである。2台のカメラは異なるシャッター速度に固定され、一方は雨滴の粒径を他方は落下速度を同じ雨滴について同時に計測する。この場合、落下速度は粒径の検定のために間欠的に参照されるので、小さい雨滴に関しても信頼度が高いのが、特徴である。

ここでは、得られた結果から2つの典型例として、ガンマー関数型分布と2山型分布のものを挙げ、これらが弱い対流と強い対流の雲からの降雨にそれぞれ対応していること示した。2山型の事例は得られたレーダの解析図と比較して議論され、熱帯特有の「暖かい雨」の形成機構として考えられる併合成長の証拠として、また雨滴の蒸発過程の可能性等が考察された。